JOURNAL OF MATERIALS RESEARCH AND TECHNOLOGY 2022;18:4427–4444

Available online at www.sciencedirect.com

jmr&t Journal of Materials Research and Technology

journal homepage: www.elsevier.com/locate/jmrt

Original Article

A novel systematic numerical approach on determination of heat source parameters in welding process

Navid Moslemi [a,*], *Soheil Gohari* [b], *Behzad Abdi* [c], *Izman Sudin* [a], *Hamidreza Ghandvar* [a], *Norizah Redzuan* [a], *Shukur Hassan* [a,d], *Amran Ayob* [a], *Sehun Rhee* [e]

[a] *School of Mechanical Engineering, Universiti Teknologi Malaysia (UTM), Skudai, 81310, Johor Bahru, Johor, Malaysia*
[b] *Department of Mechanical Engineering, The University of Melbourne, Parkville, VIC, 3010, Australia*
[c] *Department of Mechanical, Aerospace and Civil Engineering Pariser Building, The University of Manchester, United Kingdom*
[d] *Centre for Advanced Composite Materials, Office of Deputy Vice-Chancellor (Research & Innovation), Universiti Teknologi Malaysia (UTM), Skudai, 81310, Johor Bahru, Johor, Malaysia*
[e] *Division of Mechanical Engineering, Hnayang University, South Korea*

ARTICLE INFO

Article history:
Received 1 March 2022
Accepted 6 April 2022
Available online 26 April 2022

Keywords:
Heat source parameters
Artificial neural network (ANN)
Regression method
Residual stress
Pipe welding
Gas metal arc welding (GMAW)

ABSTRACT

The double-ellipsoidal heat source concept, established by Goldak, has been extensively employed to represent the energy distribution in a broad range of arc welding simulation processes. However, the Goldak's parameters need to be exactly and efficiently defined for accurate arc welding simulation. In this study, a novel procedure was proposed to accurately predict the Goldak's parameters in Gas Tungsten Arc (GTA) Welding simulation. A developed three dimensional (3D) Finite element (FE) analysis was performed to generate thirty sets of normalized input (welding pool characteristics) and outputs (Goldak's parameters). The relevance between Goldak's parameters and welding pool characteristics were established using two regression models and Artificial Neural Network (ANN) computing systems. Linear and quadratic regression models and ANN were compared for evaluation of accuracy of the parameters. Analysis of the results indicated that ANN slightly transcends both regression models, even though the regression models and ANN were able to suitably predict Goldak's parameters for welding simulation. Hence, Goldak's parameters for the welding numerical model were estimated and employed from the ANN model. 3D FE analysis based on thermal-elastic-plastic model using predicted Goldak's parameters were then conducted and validated by the experimental tests in terms of the size of welding pool, temperature distribution and induced residual stress. In the proposed procedure, the data set in training process was obtained using an efficient FE model analysis, which eliminates the cost and time associated with plenty of experimental tests.
© 2022 The Author(s). Published by Elsevier B.V. This is an open access article under the CC BY license (http://creativecommons.org/licenses/by/4.0/).

* Corresponding author.
E-mail address: moslemi.navid@utm.my (N. Moslemi).
https://doi.org/10.1016/j.jmrt.2022.04.039
2238-7854/© 2022 The Author(s). Published by Elsevier B.V. This is an open access article under the CC BY license (http://creativecommons.org/licenses/by/4.0/).

1. Introduction

Welding process has long been propounded as an essential component and structural manufacturing process in oil and gas, chemical industries, and nuclear power plants [1,2]. Girth welding of steel pipes, to manufacture and join pipeline networks, is very popular in various industries [3,4]. However, it is highly known that welding creates high amount of residual stresses [1,2,4–6]. Residual stresses, predominantly in the pipe longitudinal direction, negatively impact on structural efficiency by reducing the fatigue strength, brittle fracture or lead to stress corrosion cracking (SCC) [3]. Hence, precise prediction of residual stress behavior and structural stress analysis is of great significance to ensure integrity of welded structures [1,3,6]. Numerical modelling has been employed as a tool to predict the magnitude and distribution of residual stresses of welding structures [3,6–12]. As part of the scopes in the numerical simulation, various approximations and assumptions are essentially elucidated due to the complexity of the phenomena involved in welding processes [13].

The physical geometry and mechanical behavior of the weldment are significantly affected by the chemical–metallurgical reaction in the liquid metal, solid state phase transformation and grain growth during the welding procedure, which in turn are influenced by temperature field and thermal gradient during welding cycles [2,10,12,14]. In welding process, the generated residual stress depends on the non-uniform temperature distributions as well as the transient temperature distribution due to movement of heat sources [1]. In welding simulation, accurate temperature distribution and the following precise mechanical and metallurgical prediction in the weldment are achieved by means of a well-established thermal model [4]. Hence, outlining an appropriate thermal model marks the numerical modelling of welding processes as a rigorous duty, promptly progressing most recently [2,4,15,16]. The latest progress in numerical models provides the ability to develop and employ volumetric heat sources such as Gaussian heat source [10,17], conical heat source [2,18], and the Goldak double-ellipsoid heat source [2,19–21]. The Goldak heat source model is the most popular to date and is extensively used to predict the energy distribution in arc welding simulation process of pipe structures [19,22]. However, Goldak's model as well as other models mentioned above require that some parameters to be precisely determined because the conjunction between the parameters is significant. Assessment of the optimum Goldak's model parameters is an essential and challenging step to achieve reliable thermal gradient and temperature fields in welding simulation [5]. The issue to be addressed is how to accurately and efficiently determine the values of the parameters before welding simulation.

Some authors utilized heat source parameters from literature and this could lead to noticeable error in numerical results due to dissimilar experiment conditions [2,5]. Typically, three established methods are adopted in order to compare and verify the optimized heat source parameters:

a) Several authors [1,11,21,23–27] measured temperatures by applying thermocouples at specific points, and fitted heat source parameters in order to simulate temperature field to match the thermocouple measurements at those particular points [2,28].

b) Majority of researchers [1,10,11,24,29–31] matched the macrograph of weldment cross-section from experiment, in terms of the geometric appearance of the fusion zone (FZ), molten pool (MP) and heat affected zone (HAZ), with those from simulated results in order to iteratively determine the heat source parameters [28].

c) Some researches [1,6,9,32,33] measured residual stresses using destructive or non-destructive methods in order to simulate residual stresses in which the parameters were iteratively fitted with the measured strain–stress data [1,28].

The research reported in the references [2,34,35] emphasized the most reliable method is to adopt experimental results of temperature recording using thermocouple and observation of weldment cross-section, to verify the numerical results. Researchers [1,6,36–38] proposed verifying the simulation results with all above methods in order to assure the accuracy of mechanical as well as thermal results.

Several researchers [39–41] optimized welding process parameters by defining a mathematical model to characterize the relation between the experimental and simulation input parameters, but the procedure is costly since the time-consuming welding experiments are required to validate the prediction model. Trial and error approach has been used by many authors [42–45], however, it can be tedious and time-consuming with no guarantee that optimal parameters could be achieved [2]. Calibrated parameters of heat source using optimization approaches can significantly improve the result of welding simulation and reduce the analysis time. Various algorithms and multiple regression analysis (MRA) have been widely used to determine the parameters of welding simulation [46,47]. The MRA cannot resolve non-linear problems, however, in practice, it is extensively used with complete data for linear problems [5]. Welding heat source parameters was predicted using the partial least-squares regression analysis (PLSRA) by Jia et al. [5]. The authors [5] studied the correlation between welding pool appearance in terms of welding pool geometry and peak temperature using predicted heat source parameters by both MRA and PLSRA. Fu et al. [48] proposed an analytical method to obtain the geometry characteristic of molten pool and the temperature distribution under various welding processes. A neural-network by Levenberg–Marquardt algorithm was then used in order to train and predict the Goldak's parameters. To determine Goldak's heat source parameters, Belitzki et al. [49] proposed an image processing technique to characterize the weld seam contour, and the Genetic Algorithm (GA) and Sequential Quadratic Programming (SQP) approaches were employed to optimize the heat source parameters. Tafarroj and Kolahan [50], employed second order regression modeling and artificial neural networks (ANN) to study the correlation between welding input parameters and the Goldak's model parameters. They concluded that the ANN model performs slightly better than regression model. Various welding experiments are required in order to train the network for different welding joints using Tafarroj and Kolahan [50] method. Farias et al. [2]

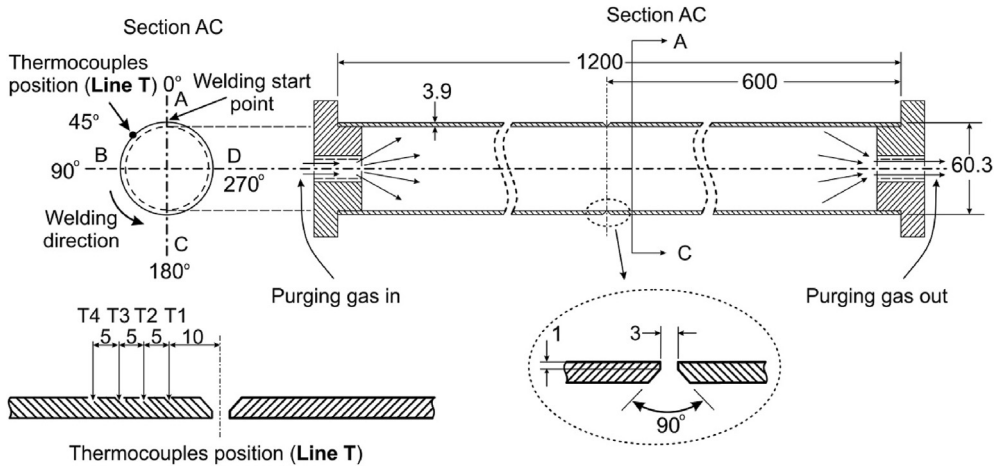

Fig. 1 – Preparation of girth-welding geometry of pipe specimen, thermocouple locations and welding direction (all dimensions are in mm).

used GA and inverse problem approaches to optimize parameters of Goldak's heat source model. The mean square of differences between the magnitude of solidus temperatures from the experimental and numerical results was considered to be the objective function in the optimization process. Hence, the optimized welding pool dimension was dependent on the objective function. Reduced Geometry procedure has been employed by authors [2] to reduce the computational time. Despite the welding pool characteristics and welding temperature profile results obtained from the FE simulation were validated with the experimental results, the FE simulation results have not been validated in terms of induced residual stress.

The review of the literature indicates the significance of heat source model associated with suitably calibrated parameters to rigorously predict the magnitude and distribution of residual stress in welding structures using FEM. However, to determine the heat source parameters, a systematic procedure is required with minimum number of time and cost consuming welding tests. In this study, a novel numerical procedure to determine Goldak's parameters using developed 3D finite element model, two regression models, and Artificial Neural Network (ANN) are proposed. The linear and quadratic regression models and neural network program based on the Levenberg–Marquardt algorithm are critically examined and compared. For this purpose, using developed FE simulation, the peak temperature (T_p) at specific points adjacent to welding zone (WZ) and size of the molten pool cross-section are acquired under numerous welding processes, using various Goldak's parameters. The FE simulation results are then used to construct regression models and to train samples of the Levenberg–Marquardt neural network. The established regression models and trained Levenberg–Marquardt neural network is finally utilized to predict the heat source parameters based on a particular double-pass welding process from a welding experiment. The numerical model developed in the current study can potentially be employed to accurately specify heat source parameters for any given welding process and ultimately eliminate the need to conduct numerous experimental tests, which can be beneficial when both time and cost reductions are sought.

2. Experimental apparatus and test procedures

The experimental test apparatus encompasses a welding pipe specimen made of AISI 316L stainless steel which has a broad application in the oil and gas industry. The schematic of the steel pipe specimen is shown in Fig. 1. The experimental setup associated with the welding process and the testing instruments are provided in Fig. 2. It should be noted that a weld filler material similar to the pipe specimen was utilized. The weld groove shape and the dimension are based on ASTM F 722–82 Standard (Fig. 1). The pipe specimens were welded by a

Fig. 2 – Welding process with thermocouples to record the transient temperature using the data logger.

certified welder. The welding procedures are based on Gas Tungsten Arc Welding (GTAW) method. The tests were conducted on the unconstrained specimen horizontally placed on the table. An inert gas was injected into all steel pipe specimens during welding procedures. The experiments were conducted at ambient temperature of 27 °C. Neither preheating nor post–weld heat treatment was done in the welding process. Four weld tacks (WT) were performed at A, B, C and D, as shown in Fig. 1, to minimize distortion during following welding passes. For the proper welding, the welding gap was filled by four quarter welding root pass (RP), AB, BC, CD, DA, and then followed by one full circumferential cover pass (CP) as shown in Fig. 1. More details on the welding sequences and dimensions are described in Section 6.

In this study two types of experiments were conducted to verify and to validate the numerical results. The first experiment was conducted to determine characteristics of welding pool and validate the transient thermal cycles and characteristics of welding pool with those obtained from numerical model using determined Goldak's parameters in Section 9. The transient thermal cycles during the welding process were recorded by thermocouples (K-type Chromel-Alumel) which were spot welded at four locations, on the outer surface at 45° from the welding start location as illustrated in Fig. 1. The temperature measurements were logged onto a data logger with a time increment of 1 s. The recorded transient temperature profiles are used to validate with numerical model in Section 6. For the purpose of detailed thermal analysis, the welding power (W) was obtained from welding parameters such as current (amps) and voltage (volts). The weld speed for the root and cover passes were measured and shown in Table 1. To observe the molten pool size of the two welding passes, the fully welded pipe specimen was transversely sectioned at 45° from the welding start location. The transverse section of the specimen was grinded, polished and etched. An etchant solution containing 70% nitric acid (HNO_3) was used as a solution. An electro-polishing machine operating voltage at 5v for 45 s was utilized for the etching process. The finished welding cross section is shown in Fig. 3. The welding pool characteristics are used to verify and validate with numerical results in Section 9. The second welding experiment was conducted to validate the nominated welding sequence.

The second experiment was conducted to validate the residual stress with numerical FE results based on thermal-elastic-plastic model using predicted Goldak's parameters, in Section 9. The hole-drilling technique was carried out on the specimens to gauge the residual stresses on the outer surface of the welded pipe at different locations adjacent to the welding pool. The details regarding the welding residual stress measurement test are described in Section 9.

Table 1 – Welding parameters for root and cover welding passes for experimental welding process.

Heat source parameter	RP	CP
Power (W)	623	732
Efficiency (%)	80	80
Velocity (mm/s)	0.85	0.9

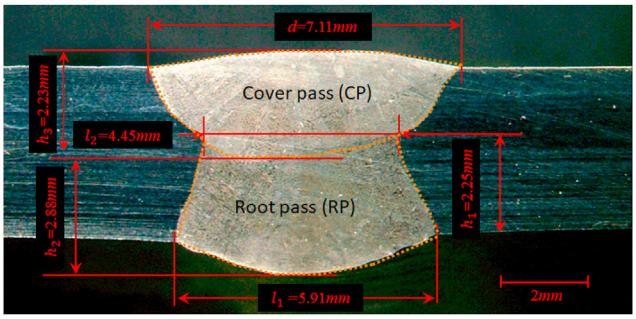

Fig. 3 – The macrograph of welding pool cross-section showing root pass (RP) and cover pass (CP), at 45° from the welding start location.

3. Double ellipsoidal moving heat source

Goldak's heat source model pertaining to the double-ellipsoidal moving heat source [34] has been broadly used for numerical simulation of the arc welding process of various metallic-based structures [2,10,11,20,21,33,36,50–54]. As such, the Goldak's double ellipsoidal moving heat source model is considered in this study for calculation of the volumetric heat flux density distribution of energy in the GMAW simulation process. The graphical configuration of Goldak's model is shown in Fig. 4. The Goldak's equations [34] can express the front and rear heat source using the following forms in Eqs. (1) and (2), respectively:

$$q_f(x,y,z,t) = \frac{6\sqrt{3}f_f Q}{a_f bc\pi\sqrt{\pi}} \exp - \left(\frac{3x^2}{a_f{}^2} + \frac{3y^2}{b^2} + \frac{z^2}{c^2}\right) \quad (1)$$

$$q_r(x,y,z,t) = \frac{6\sqrt{3}f_r Q}{a_r bc\pi\sqrt{\pi}} \exp - \left(\frac{3x^2}{a_r{}^2} + \frac{3y^2}{b^2} + \frac{z^2}{c^2}\right) \quad (2)$$

where, x, y and z correspond to the local coordinate system of the heat source model. a_r and a_f, respectively, represent the rear and the front semi-axes of the heat source model. Heat deposited fractions which are f_r and f_f , respectively, represent the rear and front parts of the model. Hence, $f_f + f_r = 2$.

Assuming the continuity of the model, $f_r = \frac{2a_r}{a_f + a_r}$ and $f_f = \frac{2a_f}{a_f + a_r}$ are considered [48], commonly f_f is considered slightly greater than f_r, which is attributed to the fact that the temperature gradient in the foreside leading part, is higher in comparison to the rear part. In the present study, f_f and f_r are chosen as 1.1

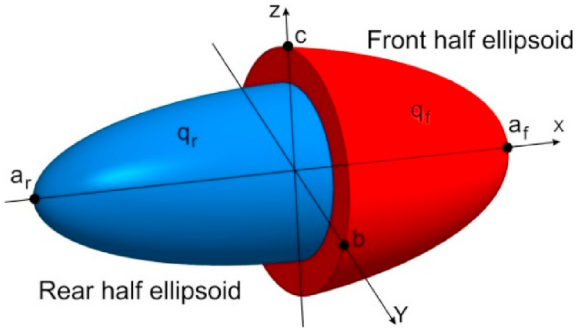

Fig. 4 – Graphical configuration of Goldak's [34] double ellipsoidal heat source model.

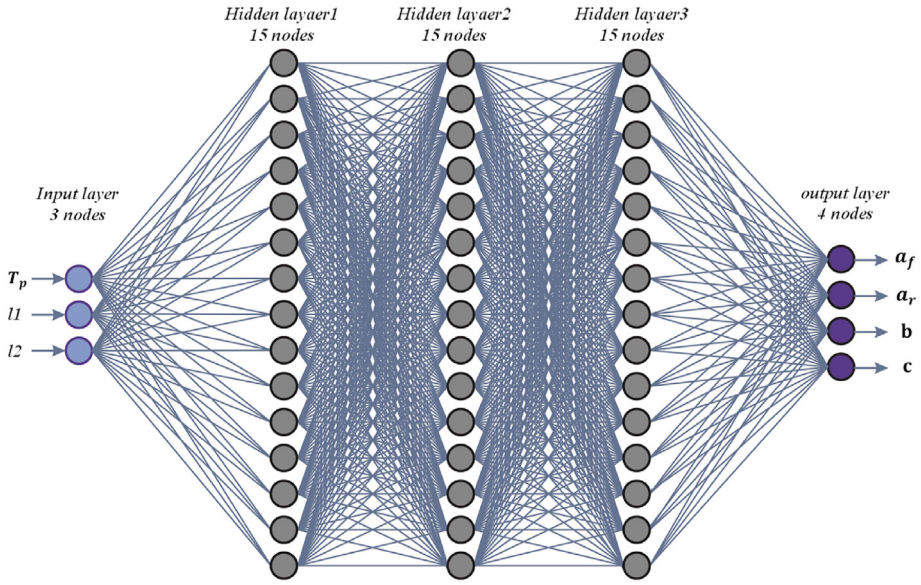

Fig. 5 – The architecture of the artificial neural network using three hidden layers.

and 0.9, respectively. If t is zero, a (i.e. a_f and a_r), b and c are the lengths which specify the profile of x_0 energy in the heat source. Q is the position of heat source in x-direction. The heat source rate, $Q = \eta VI$, is computed by means of V, where, I η, and are voltage, current and welding efficiency, respectively.

4. Mechanical analysis

The calculation of residual stresses is dependent on the former thermal analysis outcome associated with temperature distribution. The decomposition of the strain rate ($\dot{\varepsilon}_T$) into three strain components is based on Eq. (3) [1]:

$$\dot{\varepsilon}_T = \dot{\varepsilon}_E + \dot{\varepsilon}_P + \dot{\varepsilon}_{ts} \quad (3)$$

where, $\dot{\varepsilon}_E$, $\dot{\varepsilon}_p$ and $\dot{\varepsilon}_{ts}$ stand for the elastic strain rate, plastic strain rate, and thermal strain rate, respectively. The calculation of $\dot{\varepsilon}_E$ depends on the material Young's modulus and Poisson's ratio which are temperature subordinate. $\dot{\varepsilon}_{ts}$ is computed by means of temperature dependent coefficient of thermal expansion. A rate independent plastic model is employed to calculate $\dot{\varepsilon}_p$ based on Von Mises yield surface, linear kinematic hardening model and temperature-dependent stress relaxation due to visco-plastic effects. It must be noted that hardening recovery is neglected if isotropic hardening model is used. The numerical model can grant a

Table 2 – Thermal, physical and mechanical properties of AISI 316L stainless steel [1,57].

Temp °C	Specific heat kJ/kg/°C	Heat transfer coefficients W/ m^2/K	Conductivity W/m/°C	Thermal Exp. * 10^6 mm/mm/°C	Elastic Modulus, GPa
20	0.488	–	14.12	14.56	171
100	0.502	13.57	15.26	15.39	165
200	0.520	17.67	16.69	16.21	157.5
300	0.537	21.96	18.11	16.86	150
400	0.555	27.08	19.54	17.37	142.5
500	0.572	33.34	20.96	17.78	135
600	0.589	40.98	22.38	18.12	127.5
700	0.589	50.19	23.81	18.43	120
800	0.589	61.18	25.23	18.72	109
900	0.589	74.13	26.66	18.99	96.9
1000	0.589	89.21	28.08	19.27	83
1100	0.589	106.6	29.50	19.53	64.4
1200	0.589	126.48	30.93	19.79	47.3
1300	0.589	149.01	32.35	20.02	25
1400	0.589	174.37	33.78	20.21	1.7
1500	0.589	202.74	33.78	20.21	1.7
1600	0.589	234.28	33.78	20.21	1.7
1700	0.589	269.17	33.78	20.21	1.7
1800	0.589	307.57	33.78	20.21	1.7
2000	0.589	395.64	33.78	20.21	1.7

Table 3 – Tensile properties of AISI 316L stainless steel [57].

Plastic strain (%)	0	0.2	1	2	5	10
Temp °C	*True stress (MPa)*					
23	210	238	292	325	393	494
275	150	173.7	217	249	325	424
550	112	142.3	178	211	286	380
750	95	114.7	147	167	195	216
800	88	112	120	129	150	169
900	69	70	71	73	76	81
1100	22.4	23.4	24.4	25.4	26.4	27.4
1400	2.7	3.7	4.7	5.7	6.7	7.7

tensile part of loading-unloading, nevertheless, when the material is subjected to both loading-unloading during the welding process, the stresses exceed the yield point. The stress then decreases continuously and the yield point in compression is equal to the last tensile stress. The isotropic hardening model is then incapable of demonstrating the Bauschinger's effect during the inverse loading, resulting in overestimating the value of residual stress [1,7,55,56]. According to kinematic hardening model, the entire stress range is equivalent to twice the yield stress which is under the assumption that the Bauschinger's effect is present. As such, the kinematic hardening model is employed in this study which is a suitable option for numerical simulation of the welding residual stress.

5. Modeling for Goldak's parameters determination

In this section the relationship between Goldak's parameters (a_f, a_r, b, c) and welding pool characteristics (l_1, l_2 (Fig. 3) and pick temperature (T_p) at T_1 (Fig. 1)), obtained from developed FE analysis, for root pass are modeled using linear regression, quadratic regression and ANN models. Thirty sets of normalized input (welding pool characteristics) and outputs (Goldak's parameters) are provided, in Section 6. The performance of the models are critically examined and compared (Section 8), in terms of accuracy of Goldak's parameters prediction. The model which outperformed others is then employed to determine the Goldak's parameters for root and cover welding passes based on welding pool characteristics obtained from Section 2. All models are constructed and analyzed using Matlab® software. A 3D FE analyses based on thermal-elastic-plastic approach using predicted Goldak's parameters were then carried out to be verified and validated with experiment tests in terms of welding pool characteristic, temperature distribution and induced residual stress obtained in Section 9. The nominated model, in terms of accuracy, is employed to determine the Goldak's parameters for CP using similar procedure which was adopted for RP. Hence, welding pool characteristics (d_3, h (Fig. 3) and pick temperature (T_p) at T_1 (Fig. 1)) concerning the Goldak's parameters (a_f, a_r, b, c) are assumed for CP.

Table 4 – Determined heat source parameters range for thermal simulation.

Heat source parameter	Root Pass (RP)	Cover Pass (CP)
a_f (mm)	1.6–5.2	1.1–4.2
a_r (mm)	2.6–6.1	0.5–3.1
b (mm)	1.3–4.1	5.1–9.5
c (mm)	1.2–3.1	0.1–3.1

5.1. The multiple regression model

Regression analysis is a mathematical form which explains and approximates a function between one element, which is assumed as dependent variable, and further independent variables [50,58,59]. The regression analysis is generally comprised of linear and non-linear regression in which the mathematical relation between the consecutive dependent variable and the independent variables is commonly achieved by considering linear and nonlinear relationship, respectively [58]. The objective is to determine the relationship between Goldak's parameters (a_f, a_r, b, d, c) and welding pool characteristics, l_1 and l_2 (Fig. 3) and pick temperatures (T_p) at T_1 (Fig. 1) for root pass (Fig. 1) which are respectively considered as dependent and independent variables.

In the present study, two well established regression models, linear [5] and second order non-linear regression (known as quadratic regression) models were considered and assessed. The full mathematical equations of linear and quadratic regression models for the problem can be described by Eqs. (4) and (5), respectively.

$$f_{\ell,i}(l_1, l_2, T_p) = \beta_{0_i} + \beta_{1_i} l_1 + \beta_{2_i} l_2 + \beta_{3_i} T_p + \beta_{4_i} l_1 l_2 + \beta_{5_i} l_1 T_p + \beta_{6_i} l_2 T_p + \beta_{7_i} l_1 l_2 T_p \tag{4}$$

$$f_{q,i}(l_1, l_2, T_p) = \beta_{0_i} + \beta_{1_i} l_1 + \beta_{2_i} l_2 + \beta_{3_i} T_p + \beta_{4_i} l_1 l_2 + \beta_{5_i} l_1 T_p + \beta_{6_i} l_2 T_p + \beta_{7_i} {l_1}^2 + \beta_{8_i} {l_2}^2 + \beta_{9_i} {T_p}^2 \tag{5}$$

where, subscripts $f_{l,i}(l_1, l_2, T_p)$ and $f_{q,i}(l_1, l_2, T_p)$ are Goldak's parameters, and q respectively represent linear and quadratic regression models, i depicts Goladak's parameters at various welding conditions and β_{0_i}, β_{1_i}, β_{2_i}, β_{3_i}, β_{4_i}, β_{5_i}, β_{6_i}, β_{7_i}, β_{8_i}, β_{9_i} represent the regression model coefficients. The coefficients can be computed by applying multiple linear and non-linear regression algorithm associating Eqs. (4) and (5) with the simulation data series obtained from Section 6.

5.2. Artificial neural networks (ANN) model

In the present study, a multi-layer, feed-forward, back-propagation artificial neural network was employed to determine the functional correlation between the welding pool characteristics as input and the Goldak parameters as output of the network. The well-established and desirable Levenberg–Marquardt (LM) [50,60–62] training method was employed to train the ANN network. The LM algorithm is extensively used to solve problems of nonlinear least squares

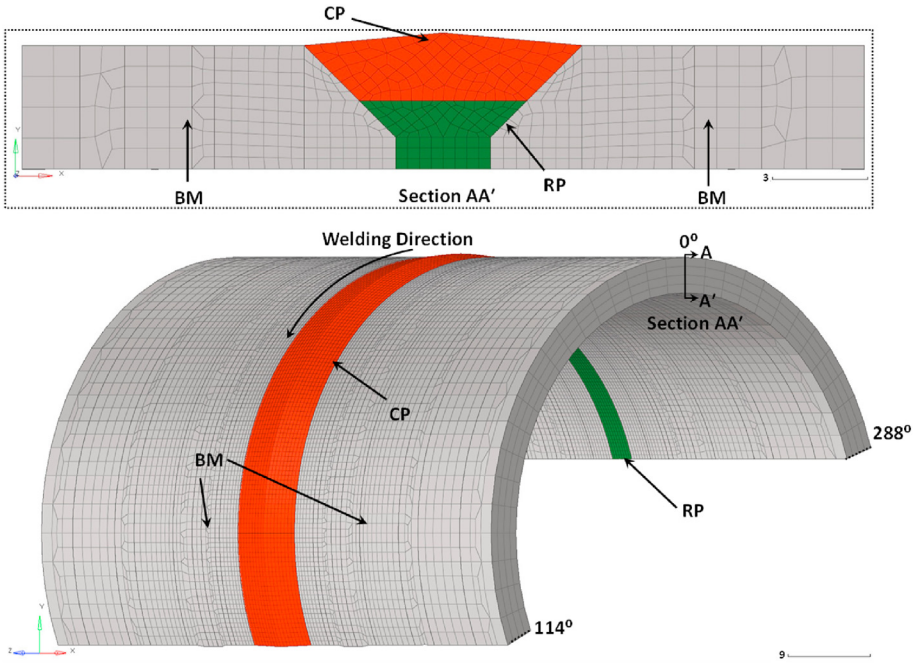

Fig. 6 – Finite element model meshing of the reduced geometry to determine Goldak's parameters.

minimization by providing a numerical solution. A description for LM algorithm is provided in the following paragraphs.

The objective function $U(x)$, which is supposed to be minimized with proportion to the vector x, is the sum of squares of nonlinear functions [63]:

$$U(x) = \tfrac{1}{2}\sum_{i=1}^{n} e_i^2(x), \tag{6}$$

where the vector $x = (x_1, x_2, \ldots, x_m)$, e_i is referred to error and called residual and each e_i would be a smooth function from $\Re^m$ to $\Re$ assuming that $n \geq m$. For simplification, the residual vector e of n components, $\Re^m \rightarrow \Re^n$, defined by the vector $e(x) = (e_1(x), e_2(x), \ldots, e_n(x))$. Eq. (6), can be then rewritten as $U(x) = \tfrac{1}{2}\, e(x)^2$. Adopting Jacobian matrix, J, of e with respect to x, the derivatives of U can be given as [64,65]:

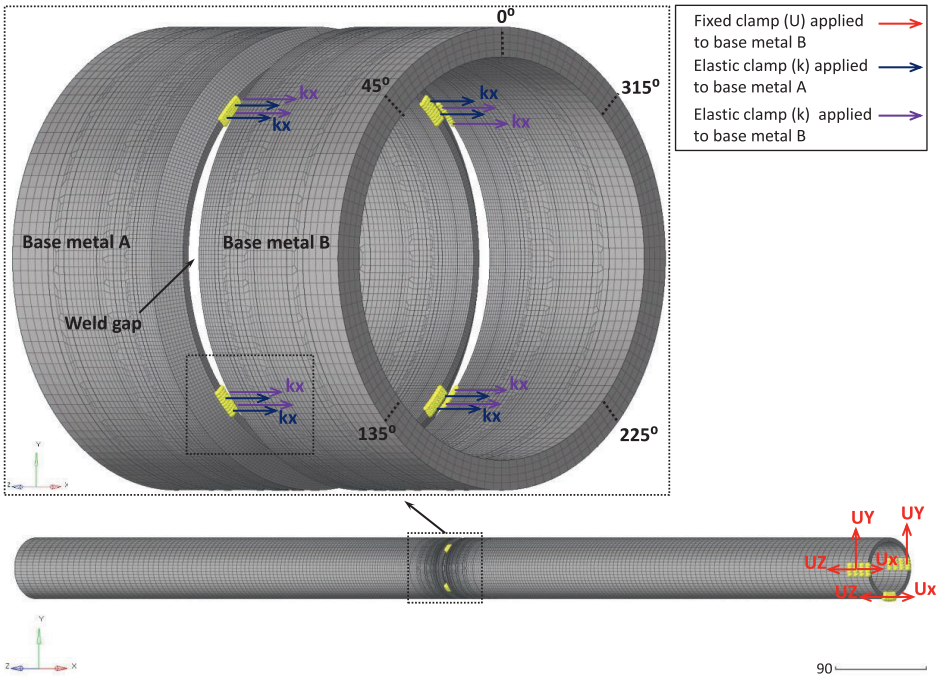

Fig. 7 – Finite element model of welding specimen showing boundary condition.

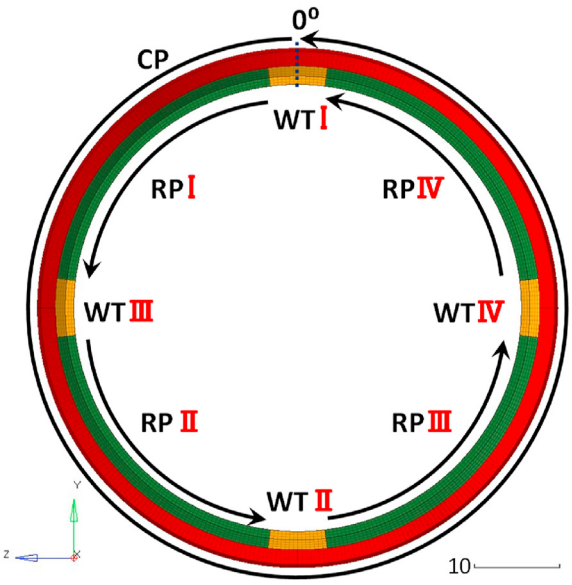

Fig. 8 – Quarter welding sequence of weld tacks (WT), root passes (RPs) and full circumferential welding of cover pass (CP).

$$J(x)=\left[\frac{\partial_{e_i}}{\partial_{x_j}}\right]_{i=1,\ldots,\ n\ and\ j=1,\ldots,\ m}=\begin{bmatrix}\frac{\partial_{e_1(x)}}{\partial_{x_1}} & \frac{\partial_{e_1(x)}}{\partial_{x_2}} & \cdots & \frac{\partial_{e_1(x)}}{\partial_{x_m}}\\ \frac{\partial_{e_2(x)}}{\partial_{x_1}} & \frac{\partial_{e_2(x)}}{\partial_{x_2}} & \cdots & \frac{\partial_{e_2(x)}}{\partial_{x_m}}\\ \vdots & \vdots & \ddots & \vdots\\ \frac{\partial_{e_n(x)}}{\partial_{x_1}} & \frac{\partial_{e_n(x)}}{\partial_{x_2}} & \cdots & \frac{\partial_{e_n(x)}}{\partial_{x_m}}\end{bmatrix} \quad (7)$$

$$=\begin{bmatrix}\nabla e_1(x)^T\\ \nabla e_2(x)^T\\ \vdots\\ \nabla e_n(x)^T\end{bmatrix}.$$

In general for non-linear problem, the gradient and Hessian of objective can be presented, respectively, in terms of $J(x)$ as follows [48,63]:

$$\nabla U(x)=\sum_{i=1}^{n} e_i(x)\nabla e_i(x)=J(x)^T e(x), \quad (8)$$

$$\nabla^2 U(x)=\sum_{i=1}^{n}\nabla e_i(x)\nabla e_i(x)^T+\sum_{i=1}^{n} e_i(x)\nabla^2 e_i(x)$$

$$=J(x)^T J(x)+\sum_{i=1}^{n} e_i(x)\nabla^2 e_i(x). \quad (9)$$

In the Gauss-Newton method, $\nabla^2 U(x)$ is approximated by the first term only in case the residual is exceedingly near the solution, hence the terms $\nabla^2 e_i(x)$ is small and can be eliminated. This can efficiently save a large amount of computational time. The Newton's method based on $U(x_j)$ and in terms of gradient and Hessian of $U(x_j)$ could be written as follows [48]:

$$x_{j+1}=x_j-\left(\nabla^2 U(x_j)\right)^{-1}\nabla U(x_j) \quad (10)$$

By substituting Eqs. (8) and (9) in Eq. (10) and assuming $\nabla^2 U(x)$ by first term only, the Gauss-Newton method can be written as:

$$x_{j+1}=x_j-\left[J(x_j)^T J(x_j)\right]^{-1} J(x_j)^T e(x_j). \quad (11)$$

The Gauss-Newton method of adopting the quadratic approximation is unable to reasonably answer the large residuals and its performance is satisfactory only for small residual problems.

Vanilla gradient descent, also called as steepest descent, is a simple optimization technique to achieve a minimum value in a function. In this method parameter optimization is carried out by stepping up the negative gradient of the function at each step. The iteration form of this method is [63,64]:

$$x_{j+1}=x_j-\mu\nabla U(x_j), \quad (12)$$

The parameter μ is a floating learning rate which should be calibrated in the following iteration based on the error in the

Table 5 – Results from ANOVA method of the linear and quadratic regression models.

Goldak's Parameters	Linear regression						Quadratic regression					
	Item	P-value	R^2	$R^2_{Adj.}$	F-value	Critical Value at 0.05	Item	P-value	R^2	$R^2_{Adj.}$	F-value	Critical Value at 0.05
a_f	l_2	0.0006	0.92	0.91	77	2.76	l_2	0.0008	0.93	0.91	77	2.76
	l_1l_2	0.0017					T_p	<0.0001				
	l_2T_p	0.0004					l_1l_2	0.0013				
	$l_1l_2T_p$	0.0016					l_1^2	0.0016				
a_r	l_2	<0.0001	0.80	0.78	35	2.98	l_1T_p	<0.0001	0.76	0.73	27	2.98
	l_1T_p	<0.0001					l_2T_p	<0.0001				
	l_2T_p	<0.0001					l_2^2	<0.0001				
b	l_2	<0.0001	0.88	0.86	62	2.98	l_1T_p	<0.0001	0.92	0.91	73	2.76
	l_1T_p	<0.0001					l_2T_p	<0.0001				
							l_1l_2	<0.0001				
	l_1l_2	<0.0001					l_1^2	<0.0001				
c	l_2	0.0027	0.78	0.75	30	2.98	l_1T_p	<0.0001	0.76	0.73	28	2.98
	T_p	<0.0001					l_2T_p	<0.0001				
	l_1T_p	<0.0001					l_2^2	0.023				

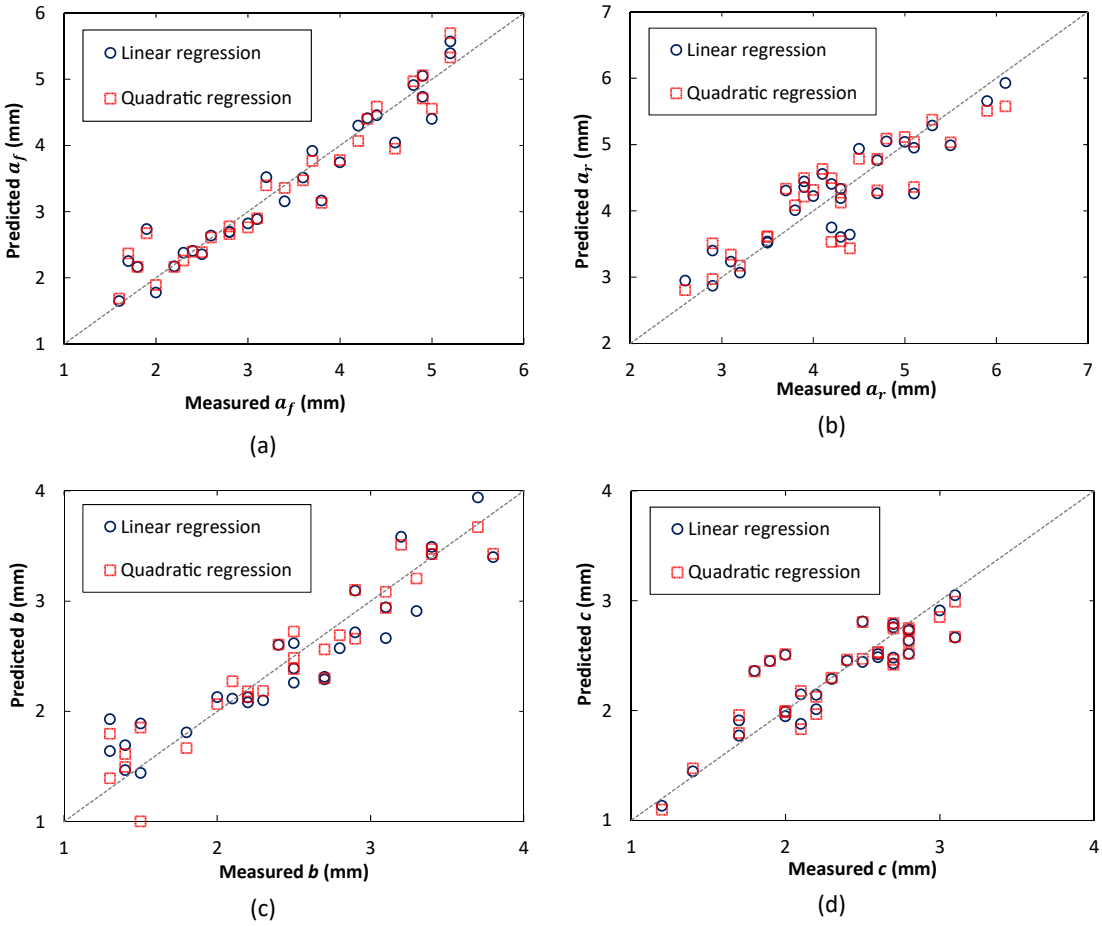

Fig. 9 – Comparison of Goldak's parameters (a) a_f (b) a_r (c) b (d) c, between measured values and predicted values.

former one. In contrary to the Gauss-Newton procedure, the descent method converges to the solution rapidly for large residual problems. However its approach to solution is significantly slow for small residual problems. To overcome the above mentioned issues with both gradient descent and Gauss-Newton algorithms, Levenberg suggested an algorithm by blending both algorithms to derive the complementary advantages of them in which:

$$x_{j+1} = x_j - \left[J(x_j)^T J(x_j) + \mu I\right]^{-1} J(x_j)^T e(x_j), \quad (13)$$

μ can be calibrated via multiplying by a factor (Υ), Υ is assumed commonly as 10, in which if the error was reduced in the former iteration, μ should be reduced by Υ so as to reduce the performance of the gradient descent method. Likewise, the influence of gradient descent should be enhanced by Υ whenever the error becomes elevated. In other words, the Levenberg algorithm is a premier method to gradient descent and Gauss-Newton whenever μ is large and small, respectively [65].

Due to the importance of architecture of the network and deficiency of routine established guidelines to determine the proper architecture of ANN [66,67], trial and error experimentations were used in the present study. Hence, three input nodes and four output nodes were selected. Three hidden layers, for higher performance of ANN, were defined after several attempts as illustrated in Fig. 5. In the present study, the input layer consisted of three nodes, including two parameters of welding pool dimensions l_1, l_2 (Fig. 3), for root pass, plus pick temperature (T_p) at T_1 (Fig. 1) for root pass. The output layer was embraced by Goldak's parameters a_f, a_r, b and c. To train the network 4 the Levenberg–Marquardt algorithm requires 30 sets of normalized inputs and outputs to be modelled using MATLAB software. The input and output data were collected from the numerical simulation results obtained in Section 6. Seventy percent of the inputs and outputs from finite element analysis (FEA) were used for training the network. To prevent over fitting, 20% of the inputs and outputs were used for early stopping, and the rest (10%) of them were used for validation.

6. Simulation of the weld process

6.1. *Material modelling*

The present FEA simulation framework is performed on the AISI316L stainless steel pipe samples using SYSWELD® commercial software package which has an extensive database for the development of predefined material properties, the

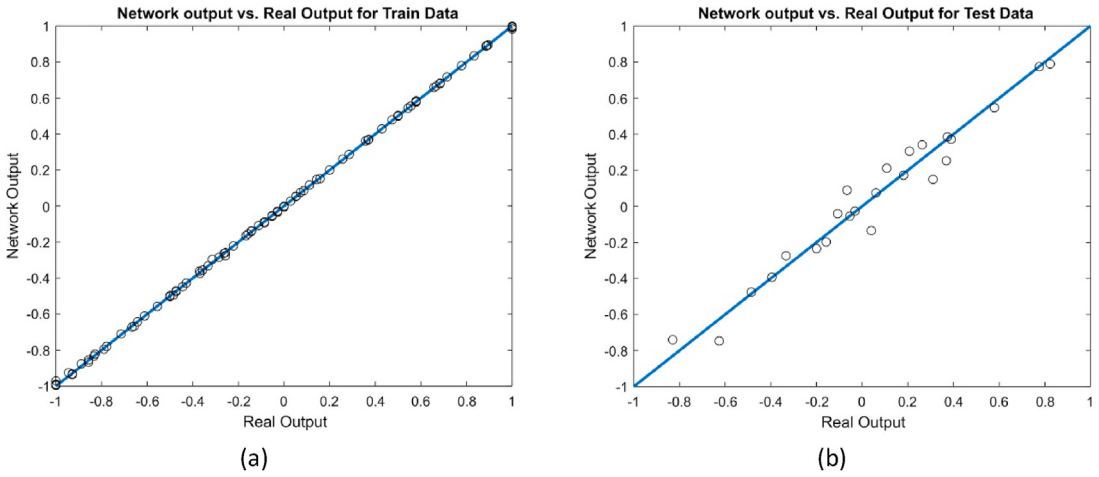

Fig. 10 – ANN output vs real output for (a) trained data, (b) test data.

thermos-metallurgical and thermos–mechanical properties. Further experimental evaluation may be required for multi-commercial materials. For higher simulation accuracy, the simultaneous effect of the thermos-physical and thermos–mechanical properties was taken into account during the simulation analysis. The various thermos-physical and mechanical properties [1,57] of AISI 316L SS for the FE simulation are shown in Table 2. The solid and liquid temperatures were assumed as 1340 °C and 1400 °C, respectively. The density was considered as 7966 kg/m^3 and Poisson's ratio as 0.294 which are temperature independent. The tensile properties at various temperatures of AISI Type 316L SS are shown in Table 3 [57].

6.2. *Finite element analysis*

In this study, the calculations of the thermal cycles and the induced residual stress are based on Goldak's heat source model [19] using SYSWELD® software package. To achieve reliable and efficient FEA models, in terms of meshing quality, the models were first generated in HYPERMESH® and then exported into SYSWELD® prior to the welding simulation process. To calculate the volumetric heat conduction, which provides the temperature profile and residual stress predictions in the weldment, quadratic 3D 8-node hexahedral (HEX8) FE elements were generated in HYPERMESH®. To further achieve higher reliability in convergence in the thermal and mechanical results, a finer mesh along the welding bead was applied while keeping elements moderately coarser away from the welding bead. A 2D element (QUAD4) in HYPERMESH®, as natural convection boundary condition on the surface of model, was generated to compute the heat transfer through convection as well as radiation to the surroundings from the weldment surface at a constant room temperature. The modeling of the weld bead geometries was extracted from the transverse section of molten pool obtained from Section 2. In the present study the chewing gum technique rather than element activation technique was

Table 6 – Input and output parameters for validation of regression models and ANN.

Set	a_f (mm)	a_r (mm)	b (mm)	c (mm)	T_p($_0$C)	l_1 (mm)	l_2 (mm)
A	4.1	3.7	2.8	2.2	680.9	4.57	5.83
B	4.5	3.2	3.3	1.8	669.9	4.68	5.82

Table 7 – Validation of developed regression models and ANN.

Goldak's Parameters	Set A			Set B		
	Linear model	Quadratic model	ANN	Linear model	Quadratic model	ANN
a_f	3.94	3.90	4.073	4.499	4.674	4.412
Relative error (%)	3.9	4.98	0.659	0.05	3.862	1.956
a_r	3.791	3.88	3.762	3.42	3.124	3.241
Relative error (%)	2.47	4.99	1.676	6.898	2.39	1.281
b	2.853	2.97	2.71	3.5	3.415	3.43
Relative error (%)	1.89	6.14	3.21	6.071	3.480	3.940
c	2.176	2.195	2.214	1.811	1.836	1.83
Relative error (%)	1.109	0.227	0.636	0.62	2.003	1.667

Table 8 – Heat source parameters as predicted by ANN.

Heat source parameter	First welding pass	Second welding pass
a_f (mm)	3.2	2.5
a_r (mm)	4.5	1.5
b (mm)	2.8	8.2
c (mm)	2.5	0.7

employed for the deposited materials as welding passes. Readers may refer to [1] which critically compared the chewing gum and element activation methods.

The numerical approach is constituted of two major steps. First, a set of 50 thermal simulations were conducted using various Goldak's parameters to obtain associated welding pool characteristics (dimensions and pick temperature). The welding pool characteristics and Goldak's parameters were then employed to evaluate regression and ANN models (as discussed in Section 5). It was observed from previous studies [5,47] that among Goldak's parameters, *bandc* intensely influence the welding pool shape characteristics (l_1, l_2 and d, h_3) in comparison to a_f and a_r. Based on the approach presented by [5,47] and in trial and error analysis, the first 20 thermal simulations, were carried out to gain the range of Goldak's parameters (a_f, a_r, *bandc*) from which the welding pool dimensions and pick temperatures were satisfactorily close to those from experiment. The ranges obtained for RP and CP are presented in Table 4. The remaining 30 thermal simulations were applied within the range given in Table 4. In order to stay within the limit of computational time, a reduced geometry of the specimen, proposed by [2], was only considered when performing the thermal analysis. A reduced geometry of the model included the Root Pass (RP), Cover Pass (CP) and Base Metal (BM), as shown in Fig. 6. As shown in Fig. 6, a shorter axial size and half circumferential of the standard model, presented in Section 2, was only considered for thermal analysis. Moreover, only a quarter of weld line from point A to B, in Fig. 1, for both root and cover passes in circumference direction were welded. The weld bead cross-section and pick temperature (T_p) were extracted at 45° from welding starting point. The data set from 30 simulated tests for RP is presented in Appendix A.

In the second step, a 3D FE analysis was conducted based on thermal-elastic-plastic approach using the predicted Goldak's parameters which were validated with experiment tests. The validation was in terms of welding pool characteristics, temperature distribution and induced residual stresses. The FE model of the pipe specimen, including boundary conditions before the start of the welding process, is shown in Fig. 7. As shown in Fig. 7, the elastic clamps (K) in X-direction were located at four positions inside the weld gap at 45°, 135°, 225°, and 315°, and the rigid constraints were applied at one end of the specimen.

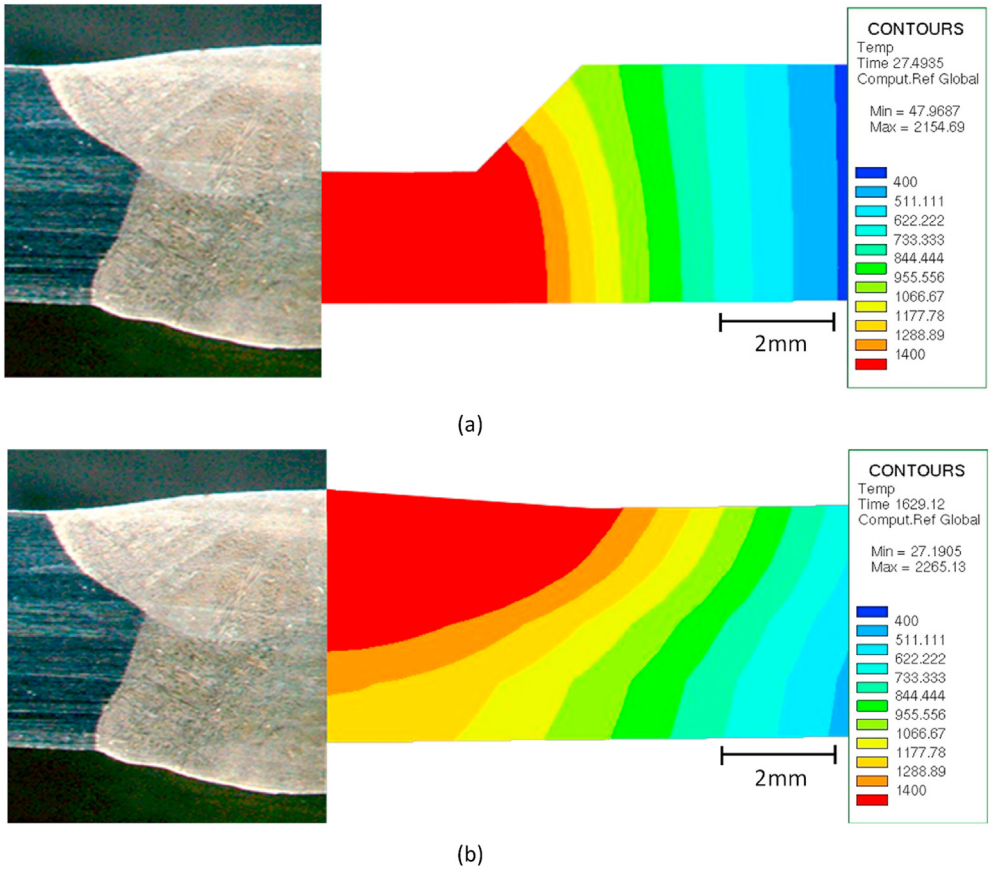

Fig. 11 – The weld pool shapes, from welding experiment and FEM, using parameters determined from ANN, (a) Root pass (RP), (b) Cover pass (CP).

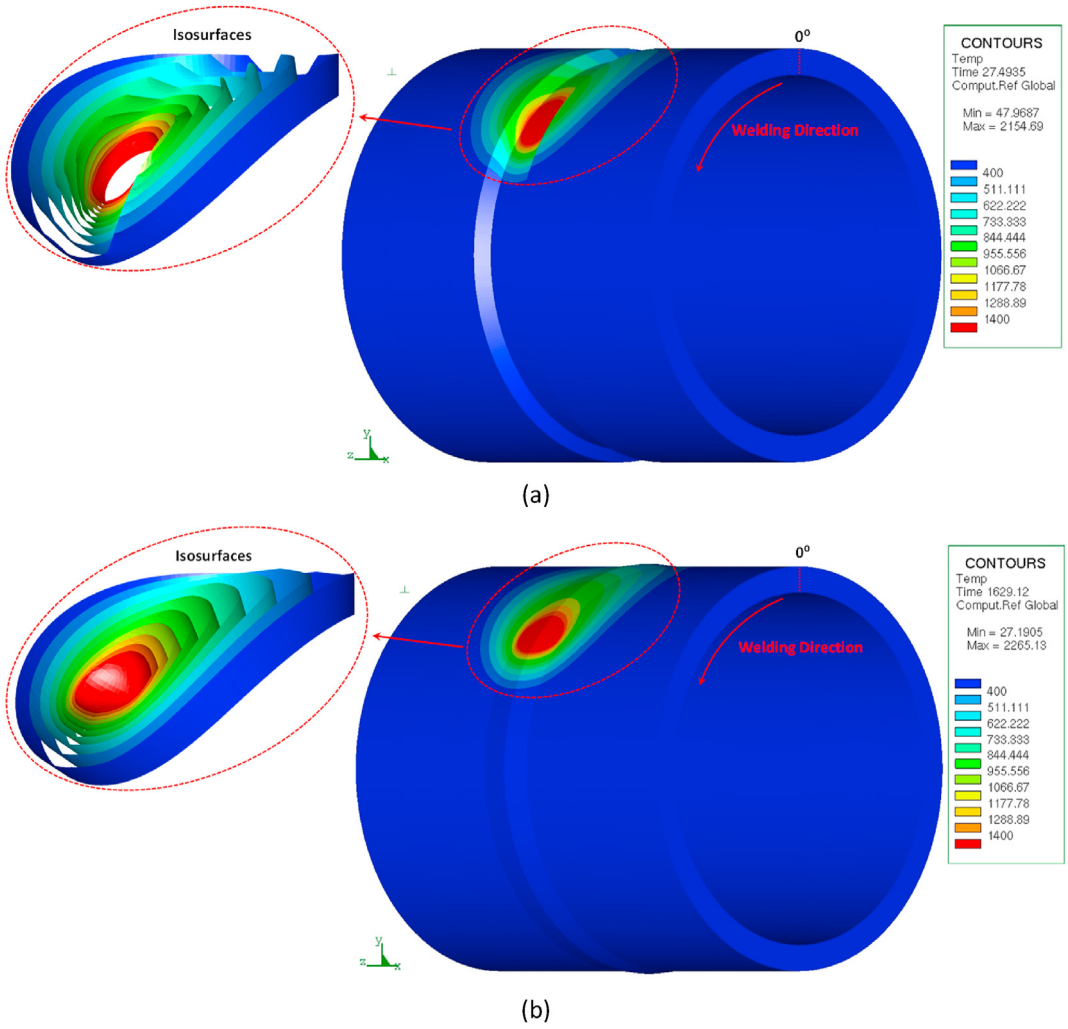

Fig. 12 – 3D temperature contour on the outer surface of pipe specimen, at 45° from welding start point, (a) Root pass (RP), (b) Cover pass (CP).

The weld gap, shown in Fig. 7, was filled with four Weld Tacks (WT) which were applied first in the sequences of WT**I**, WT**II**, WT**III** and WT **IV** followed by RPs in the order of RP**I**, RP**II**, RP**III** and RP **IV,** and finally the remaining gap was filled in with CP as shown in Fig. 8. It is to be noted that the elastic constraints were located in the middle of the weld tacks in circumferential direction to avoid welding distortion during application of the weld tacks. The elastic clamps were then removed after the weld tacks were applied, while the rigid constraints were kept until completion of the following cover pass, to prohibit rigid body motion. Hence, the weld tacks were meant to moderate distortion during welding process of the following welding passes. Once the welding simulation was carried out and the entire pipe specimen was cooled down to room temperature the results were validated by experiment tests.

7. Regression model results and discussion

The Analysis of Variance method, known as ANOVA, was carried out to evaluate the regression mod6el in terms of significance of various mathematical models obtained based on training data. For linear and quadratic regression models the significance level was considered to be 5%. The goodness of regression model is judged by the R-square and the adjusted R-square. The performance of the R-square can also be tested by evaluating the F-value. The F-value of the mathematical model is supposed to be higher than the critical value of F at the pre-determined significance level (5%). Hence, it can be concluded that the mathematical model is suitably constructed as long as the F-test is satisfied. The P-test is carried out to analyze the significance of each regression coefficient. If the P-value of each coefficient is lesser than the significance level (0.05), it can be concluded that the regression coefficient is significant enough for the construction of the regression model. Otherwise, the coefficient is near or equal to zero. In contrast to conventional regression analyses [68,69], in this study the combination of significant coefficients was determined, in which the final mathematical model for each Goldak's parameters was obtained from only those coefficients that satisfactorily passed the ANOVA test in terms of F-test and P-test. In other words, the best combination of non-zero coefficients has been determined for each Goldak's

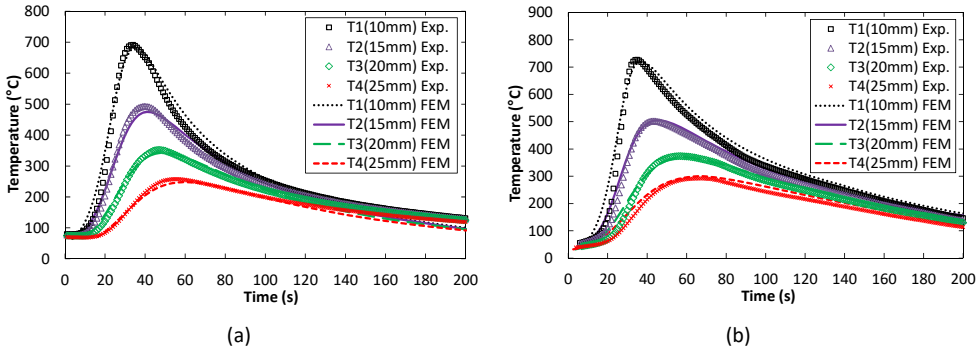

Fig. 13 – The temperature profiles from experimental and finite element simulation at different positions, (a) RP, (b) CP.

parameters. Pursuant to the results obtained from ANOVA, the linear and second order constituted models calibrated with significant regression coefficient for Goldak's parameters are presented as follows:

$$a_{f,\ell} = 8.237 + 52.151l_2 - 0.077l_2T_p - 9.966l_1l_2 + 0.0146l_1l_2T_p \quad (14)$$

$$a_{r,\ell} = 18.816 - 6.472l_2 - 0.0053l_1T_p + 0.0099l_2T_p \quad (15)$$

$$b_\ell = 32.579 - 6.854l_2 - 0.0072l_1T_p + 1.286l_1l_2 \quad (16)$$

$$c_\ell = -8.048 + 0.888l_2 + 0.0249T_p - 0.00384l_1T_p \quad (17)$$

$$a_{f,q} = 88.655 - 13.427l_2 - 0.0666T_p + 2.828l_1l_2 - 1.746{l_1}^2 \quad (18)$$

$$a_{r,q} = 0.3036 - 0.0052l_1T_p + 0.0099l_2T_p - 0.576{l_2}^2 \quad (19)$$

$$b_q = 8.779 + 0.566l_1l_2 + 0.0467l_1T_p - 0.0405l_2T_p - 6.768{l_1}^2 \quad (20)$$

$$c_q = 3.776 - 0.004l_1T_p + 0.0041l_2T_p - 0.1649{l_2}^2 \quad (21)$$

where, subscripts and q respectively represent linear and quadratic regression models. The statistical characteristics of both regression models according to ANOVA are given in Table 5. As shown in Table 5, the R-square and the adjusted R-square show that both models were satisfactory fitted to the finite element data. In particular, the suitable magnitudes of the adjusted R-squares for both models confirm that they are able to estimate the outputs of test data accurately. The averages of R-square coefficients of all predicted parameters were 0.85 and 0.84 for linear and quadratic models, respectively. The adjusted R-squares are well in compromise with the R-square for all parameters in both regression models. The averages of adjusted R-squares over Goldak's parameters for linear and quadratic models are 0.83 and 0.82, respectively. The minimum R-squares for linear and quadratic models are 0.78 and 0.76, respectively. Hence, it can be concluded the accuracy of linear model is slightly higher than quadratic model in regard to the magnitude of R-squares. The F-values for all parameters are remarkably higher than the critical value at significant level which verifies that both models were suitably created. Moreover the P-values of the all coefficients are smaller than the significance level (5%) which means that the adopted combinations of regression coefficients are significant in determining the Goldak's parameters.

Fig. 9(a-d) demonstrates the result of the predicted Goldak's parameters compared to those obtained from FEM. Note that, the hollow rings are estimated by linear model and squares shapes represent the values estimated by quadratic model. The relationship between estimated and FEM Goldak's parameters is shown in Fig. 9. The figure also highlights the high precision of estimation achieved using both mathematical

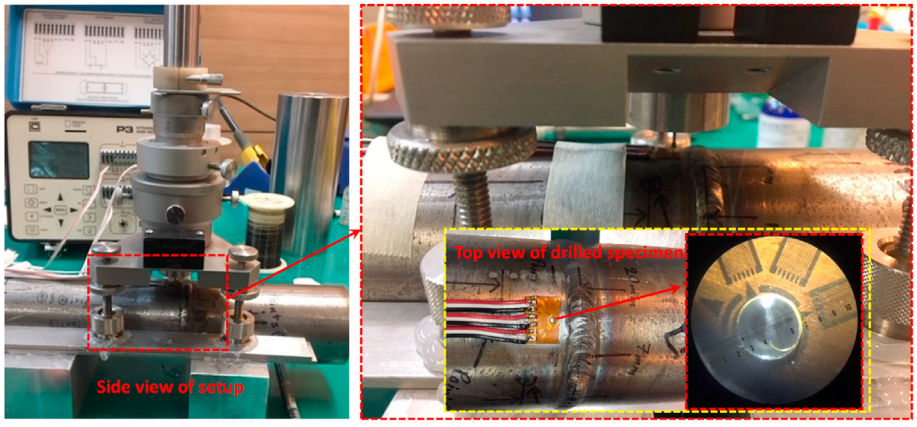

Fig. 14 – The experimental setup for hole-drilling method.

models, as shown by the predicted and measured data crossing the middle line. The accuracy of both models for all Goldak's parameters is relatively similar and no significant variances can be observed. However, the linear model is observed to be slightly better than the quadratic model in predicting *b*, which is also in agreement with the R-square value in Table 5. The performance of both regression and ANN models, in terms of relative error, is evaluated and compared using the new welding pool characteristics data in following Section.

8. Artificial neural networks (ANNs) model results and discussion

The performance of the parameters determined using ANN highly depends on the goodness and amount of the data set used in training process. Hence, the minimum number of 30 data sets was taken to assure quality of the parameters. As described in Section 6, the normalized data has been used to guarantee the goodness of data set. Determination of ANN parameters for root passes was stopped after 32 epochs with the mean-square error of 6.685e-5 and 9.235e-3 for training and validation, respectively. Figs. 10a and b demonstrate the plot of network output vs real data for training and test data of root pass, respectively. As illustrated in the figures, the errors are significantly low and the output data were satisfactorily dispersed which proves excellent ability and reliability of the network in predicting Goldak's parameters. Moreover, it can be also observed of the randomness of data.

The accuracy of the developed regression and network models was also investigated using the two new welding pool characteristics data which have not been used in the earlier processes, as shown in Table 6, and the results are provided in Table 7. From Table 7, the maximum and average value of the relative error are respectively 3.9% and 2.33% for linear regression, 6.14% and 4.08% for quadratic regression and 3.21% and 1.546% for ANN models, for the first data set. The values for the second data set are respectively 6.898% and 3.395% for linear regression, 3.862% and 2.933% for quadratic regression and 3.94% and 2.21% for ANN models. It can be concluded that, in general, the developed ANN presents the least relative error among all models and obviously outperforms both regression models. However, the regression models are created and implemented more straightforward than the neural networks. In other words, the regression model is advisable where simplicity of the parameters determination is a precedence factor; else, the developed neural network is highly proposed. Furthermore, the performance of linear model is slightly better than quadratic model for first data set and the performance of the models are reversed for second data set which demonstrates that both regression models perform relatively similar.

Following the above conclusion, the ANN method was employed to determine Goldak's parameters for cover pass (CP) as well as root pass (RP) and the results are given in Table 8. Two sets of Goldak's parameters, for root and cover welding passes, were then gathered and were eventually validated by the experiment results obtained from Section 2 and presented in following Section.

9. Goldak's parameters validation

The FE simulation, based on latest parameters (Table 8) obtained from the ANN (Section 8), was then conducted as described in Subsection 6.2. The configuration of the shape of the weld pools obtained from the experiment and FE simulation associated with both welding passes are shown in Fig. 11. The HAZ encompasses series of contours that alternated from 400 to 1400 °C. 1400 °C is the melting temperature which defines the fusion zone (FZ) of welding passes. As demonstrated in Fig. 11, the welding pool sizes from the experiment and numerical results are in good agreement for both root and cover passes. The simulation results of the 3D temperature distribution on the outer surface for the root and cover welding passes at 45° from the welding start point are presented in Figs. 12(a) and (b). The elliptical shape of temperature distribution can be observed on the outer surface of the pipe specimen for both welding passes which are in agreement with previous researches [70,71]. The profiles of transient temperature for RP and CP from experiment and simulation for different locations are compared in Figs. 13(a) and (b), respectively. From Fig. 13, the experimental and FE simulation results are in satisfactory agreement at all thermocouple locations for both welding passes. The maximum

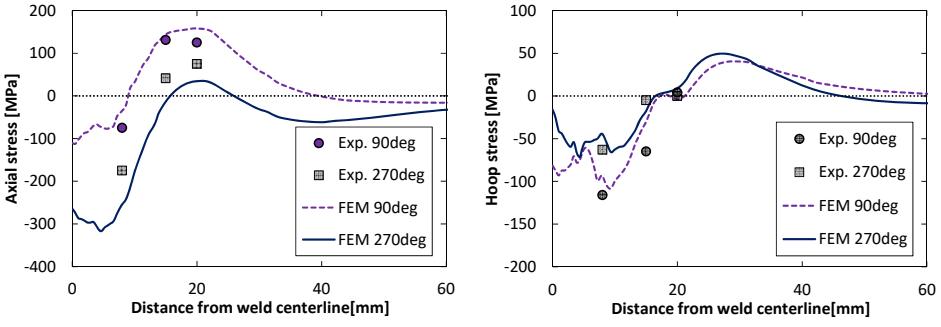

Fig. 15 – Comparison of residual stress distribution between experiment and FE simulation.

variance in peak temperatures between experimental and FE simulation results were 3.06% and 3.75% at 15 mm and 25 mm locations, respectively. The rates of increase and decrease in temperature as well as peak temperature are in favorable compromise with each other. However, during cooling from higher temperatures of both welding passes, the FE values were slightly higher than those from experiment results which indicate the heat losses in cooling period would be a little higher from those obtained by the experiment.

The residual stress distributions from FEM are procured upon cooling down the welded pipe to the ambient temperature. As described in Sections 6.2, the 3D finite element (FE) model based on thermal-elastic-plastic approach, using the predicted parameters in SYSWELD®, was employed to validate the residual stresses obtained from the welding experiment. To measure the residual stresses occurring on the outer surface of the welded pipe test specimen, the hole-drilling method was used. Detailed information regarding the determination of residual stresses using the hole-drilling method is available in the literature [72].

Since the FE simulation did not exhibit significant magnitude of radial residual stresses, the results of axial and hoop residual stresses only were considered to compare with the experimental results. The axial and hoop residual stresses on the outer surface were measured at six different locations, which is 7, 15, and 20 mm away from the weld center line and at 90° and 270° from the welding starting point. The test setup for hole-drilling technique used in the present study is shown in Fig. 14. The axial and hoop residual stress measurements from experiment and from FE simulation are plotted in Figs. 15(a) and (b), respectively. A good agreement between the experimental and FE results can be observed in terms of magnitude and trend for both axial and hoop residual stresses.

The validated FE results in terms of welding pool characteristics, temperature distribution and induced residual stress demonstrate that the developed computational procedure to determine the heat source parameters which is proposed in the present study could be employed for the investigation of induced residual stresses in multiple pass welding of AISI 316L stainless steel pipe specimen. The proposed numerical model eliminates the need to conduct various welding experiments to create input–output data sets in training regression or ANN models. This prediction technique can be trained using small normalized data sets (30–50 sets of FE input–output data). Therefore, an experimental test is only required to validate the accuracy of the predicted heat source parameters. In addition, in the proposed model, there is no limitation of welding procedure in terms of type of arc welding, welding specimen dimensions, multi-pass welding, and the heat source.

10. Concluding remarks

The main aim of this study was to introduce a new systematic approach on estimation of Goldak' parameters using the developed FE model, regression analysis, and artificial neural networks in the numerical simulation for GTAW process. The performance of linear and quadratic regression models, and ANN were critically examined and compared for accuracy of the parameters. The determined Goldak's parameters were then satisfactorily validated with the experimental results in terms of welding pool characteristics, temperature distribution and induced residual stresses. In summary, the following concluding remarks are summarized:

- The average relative errors for the first and second sets of parameters, using linear and quadratic regression models, are reliable for the purpose of predicting the Goldak's parameters.
- The average relative errors for the two sets of parameters using ANN demonstrate that the ANN model clearly outperforms both regression models. Hence, the ANN method can be confidently employed to determine the Goldak's parameters for the root and cover passes.
- The small relative error given by the regression models makes them potentially alternatives to estimate the Goldak's parameters. Notwithstanding of the fact that both regression models perform lesser against ANN, the regression models can be simply constructed and implemented, which is a significant benefit.
- The proposed procedure eliminates the necessity of performing many welding experiments in acquiring input–output data sets to train regression or ANN models.
- The prediction models can be trained using 30–50 sets of FE input–output data; hence a validation experiment set is only required to assure the accuracy of the predicted heat source parameters.
- Using the proposed procedure, there is no limitation of welding process in terms of type of arc welding, welding specimen dimensions, multi-pass welding and the heat source model.

Declaration of Competing Interest

The authors declare that they have no known competing financial interests or personal relationships that could have appeared to influence the work reported in this paper.

Acknowledgments

N.M. would like to acknowledge the funding received from UTM under the Post-Doctoral Fellowship Scheme (Grant. No. Q.J130000.21A2.05E30) for the Project: "Uniaxial and Biaxial Ratcheting of a Girth-Welded Super Duplex Stainless Steel (UNS S32750) Pressurized Pipe".

Appendix A. Obtained data set of RP for regression models and ANN.

The data set of Goldak's parameters with associated welding pool characteristics (l_1 and l_2 and pick temperature (T_p)) for root pass (RP) are presented in following table.

Sets	a_f(mm)	a_r(mm)	b(mm)	c(mm)	T_p (^{0}C)	l_1(mm)	l_2(mm)
1	2.6	3.7	2.1	1.8	699.5	4.62	6.05
2	2.8	3.9	2.2	1.9	698.3	4.57	6
3	3	4.1	2.3	2	696.7	4.51	5.91
4	3.4	4.3	2.5	2.2	689.4	4.73	6.22
5	3.8	4.7	2.7	2.4	690.9	4.55	6
6	4.2	5.1	2.9	2.6	678	4.4	5.72
7	4.6	5.5	3.1	2.8	685.3	4.24	5.34
8	5	5.9	3.3	3	684.2	4.02	5.01
9	5.2	6.1	3.4	3.1	674.4	3.85	4.79
10	4.9	3.1	3.2	1.7	664.8	4.57	5.67
11	4.3	3.5	2.9	2.1	673.2	4.57	5.86
12	3.7	4	2.4	2.5	682.1	4.46	5.8
13	3.1	4.3	2	2.8	693.9	4.57	6.11
14	2.2	5	1.4	2.8	704.7	4.46	5.92
15	1.9	5.1	1.3	2.8	697.3	4.4	5.83
16	1.6	5.3	1.4	2.7	712.3	4.46	5.89
17	2.4	4.7	1.8	3.1	700.8	4.51	6.05
18	2.8	4.3	2.2	2.7	696.6	4.65	6.22
19	3.2	4.2	2.5	2.6	687.3	4.46	5.83
20	3.6	3.8	2.8	2.3	686.8	4.57	5.91
21	4	3.5	3.1	2	683	4.67	5.9
22	4.4	3.2	3.4	1.7	671.3	4.68	5.78
23	4.8	2.9	3.7	1.4	666.6	4.68	5.45
24	5.2	2.6	4.1	1.2	664.4	4.62	4.95
25	4.9	2.9	3.8	2	670	4.57	5.67
26	1.7	3.9	1.5	2.7	703	4.68	6.33
27	1.8	4.8	1.3	2.7	703.7	4.46	6
28	2	4.5	1.5	2.5	707.3	4.57	6.33
29	2.3	4.4	2.7	2.1	710	4.95	6.44
30	2.5	4.2	2.5	2.2	707.3	4.9	6.44

REFERENCES

[1] Moslemi N. Ratcheting assessment of AISI 316L stainless steel welded pipe joint. Universiti Teknologi Malaysia; 2019.

[2] Farias R, Teixeira P, Vilarinho L. An efficient computational approach for heat source optimization in numerical simulations of arc welding processes. J Constr Steel Res 2021;176:106382.

[3] Hemmatzadeh M, Moshayedi H, Sattari-Far I. Influence of heat input and radius to pipe thickness ratio on the residual stresses in circumferential arc welded pipes of API X46 steels. Int J Pres Ves Pip 2017;150:62–71.

[4] Mirzaee-Sisan A, Wu G. Residual stress in pipeline girth welds-A review of recent data and modelling. Int J Pres Ves Pip 2019;169:142–52.

[5] Jia X, Xu J, Liu Z, Huang S, Fan Y, Sun Z. A new method to estimate heat source parameters in gas metal arc welding simulation process. Fusion Eng Des 2014;89:40–8.

[6] Ravisankar A, Velaga SK, Rajput G, Venugopal S. Influence of welding speed and power on residual stress during gas tungsten arc welding (GTAW) of thin sections with constant heat input: a study using numerical simulation and experimental validation. J Manuf Process 2014;16:200–11.

[7] Moslemi N, Mozafari F, Abdi B, Gohari S, Redzuan N, Burvill C, et al. Uniaxial and biaxial ratcheting behavior of pressurized AISI 316L pipe under cyclic loading: experiment and simulation. Int J Mech Sci 2020;179:105693.

[8] Venkateswarlu K, Kumar PN, Ravikumar P. Finite element simulation of temperature distribution, distortion and residual stresses of dissimilar welded joints. Mater Today Proc 2018;5:11933–40.

[9] Ren S, Li S, Wang Y, Deng D, Ma N. Finite element analysis of residual stress in 2.25 Cr-1Mo steel pipe during welding and heat treatment process. J Manuf Process 2019;47:110–8.

[10] Attar MA, Ghoreishi M, Beiranvand ZM. Prediction of weld geometry, temperature contour and strain distribution in disk laser welding of dissimilar joining between copper & 304 stainless steel. Optik 2020;219:165288.

[11] Ghafouri M, Ahn J, Mourujärvi J, Björk T, Larkiola J. Finite element simulation of welding distortions in ultra-high strength steel S960 MC including comprehensive thermal and solid-state phase transformation models. Eng Struct 2020;219:110804.

[12] Hemmesi K, Mallet P, Farajian M. Numerical evaluation of surface welding residual stress behavior under multiaxial mechanical loading and experimental validations. Int J Mech Sci 2020;168:105127.

[13] Knoedel P, Gkatzogiannis S, Ummenhofer T. Practical aspects of welding residual stress simulation. J Constr Steel Res 2017;132:83–96.

[14] Fu G, Lourenço MI, Duan M, Estefen SF. Influence of the welding sequence on residual stress and distortion of fillet welded structures. Mar Struct 2016;46:30–55.

[15] Smith MC, Smith AC. Advances in weld residual stress prediction: a review of the NeT TG4 simulation round robin part 1, thermal analyses. Int J Pres Ves Pip 2018;164:109–29.

[16] Smith MC, Smith AC. Advances in weld residual stress prediction: a review of the NeT TG4 simulation round robins part 2, mechanical analyses. Int J Pres Ves Pip 2018;164:130–65.

[17] Zhao X, Wang K. Finite element simulation of the residual stress in Ti6Al4V titanium alloy laser welded joint. Int J Mater Res 2019;110:466–75.

[18] Wu C, Wang H, Zhang Y. A new heat source model for keyhole plasma arc welding in FEM analysis of the temperature profile. Weld. J. New York 2006;85:284.

[19] Goldak J, Chakravarti A, Bibby M. A new finite element model for welding heat sources. Metall Trans A B 1984;15:299–305.
[20] Ni J, Wang X, Gong J, Wahab MA. Thermal, metallurgical and mechanical analysis of circumferentially multi-pass welded P92 steel pipes. Int J Pres Ves Pip 2018;165:164–75.
[21] Vakili-Tahami F, Majnoun P, Ziaei-Asl A. Controlling the in-service welding parameters for T-shape steel pipes using neural network. Int J Pres Ves Pip 2019;175:103937.
[22] Fu G, Lourenco MI, Duan M, Estefen SF. Effect of boundary conditions on residual stress and distortion in T-joint welds. J Constr Steel Res 2014;102:121–35.
[23] Aloraier AS, Joshi S. Residual stresses in flux cored arc welding process in bead-on-plate specimens. Mater Sci Eng, A 2012;534:13–21.
[24] Hildebrand J. Numerical welding simulation-Determination of temperature, microstructure and residual stress in welded joints of steel and glass materials (Numerische Schweißsimulation-Bestimmung von Temperatur, Gefüge und Eigenspannung an Schweißverbindungen aus Stahl-und Glaswerkstoffen). Verlag der Bauhaus-Universität Weimar; 2009.
[25] Chen B-Q, Hashemzadeh M, Soares CG. Numerical and experimental studies on temperature and distortion patterns in butt-welded plates. Int J Adv Manuf Technol 2014;72:1121–31.
[26] Shim Y, Feng Z, Lee S, Kim D, Jaeger J, Papritan J, et al. Determination of residual stresses in thick-section weldments. Weld J 1992;71:305–12.
[27] Zhang Y, Wang Y. The influence of welding mechanical boundary condition on the residual stress and distortion of a stiffened-panel. Mar Struct 2019;65:259–70.
[28] Joshi S, Hildebrand J, Aloraier AS, Rabczuk T. Characterization of material properties and heat source parameters in welding simulation of two overlapping beads on a substrate plate. Comput Mater Sci 2013;69:559–65.
[29] Belhadj A, Bessrour J, Masse J-E, Bouhafs M, Barrallier L. Finite element simulation of magnesium alloys laser beam welding. J Mater Process Technol 2010;210:1131–7.
[30] Dong Z, Wei Y. Three dimensional modeling weld solidification cracks in multipass welding. Theor Appl Fract Mech 2006;46:156–65.
[31] Saravanan S, Sivagurumanikandan N, Raghukandan K. Effect of heat input on microstructure and mechanical properties of Nd: YAG laser welded super duplex stainless steel-Numerical and experimental approach. Optik 2019;185:447–55.
[32] Price JW, Ziara-Paradowska A, Joshi S, Finlayson T, Semetay C, Nied H. Comparison of experimental and theoretical residual stresses in welds: the issue of gauge volume. Int J Mech Sci 2008;50:513–21.
[33] Dehkordi YG, Anaraki AP, Shahani AR. Study of the effective parameters on welding residual stress relaxation in aluminum cylindrical shells under cyclic pressure. Thin-Walled Struct 2019;143:106235.
[34] Goldak JA, Akhlaghi M. Computational welding mechanics. Springer Science & Business Media; 2005.
[35] Flint T, Francis J, Smith M, Balakrishnan J. Extension of the double-ellipsoidal heat source model to narrow-groove and keyhole weld configurations. J Mater Process Technol 2017;246:123–35.
[36] Rikken M, Pijpers R, Slot H, Maljaars J. A combined experimental and numerical examination of welding residual stresses. J Mater Process Technol 2018;261:98–106.
[37] Velaga SK, Ravisankar A. Finite element based parametric study on the characterization of weld process moving heat source parameters in austenitic stainless steel. Int J Pres Ves Pip 2017;157:63–73.
[38] Chukkan JR, Vasudevan M, Muthukumaran S, Kumar RR, Chandrasekhar N. Simulation of laser butt welding of AISI 316L stainless steel sheet using various heat sources and experimental validation. J Mater Process Technol 2015;219:48–59.
[39] Tarng Y, Yang W, Juang S. The use of fuzzy logic in the Taguchi method for the optimisation of the submerged arc welding process. Int J Adv Manuf Technol 2000;16:688–94.
[40] Tarng Y, Juang S, Chang C. The use of grey-based Taguchi methods to determine submerged arc welding process parameters in hardfacing. J Mater Process Technol 2002;128:1–6.
[41] Li P, Lu H. Hybrid heat source model designing and parameter prediction on tandem submerged arc welding. Int J Adv Manuf Technol 2012;62:577–85.
[42] Gao X, Wu C, Goecke S-F, Kügler H. Numerical simulation of temperature field, fluid flow and weld bead formation in oscillating single mode laser-GMA hybrid welding. J Mater Process Technol 2017;242:147–59.
[43] Jiang W, Chen W, Woo W, Tu S-T, Zhang X-C, Em V. Effects of low-temperature transformation and transformation-induced plasticity on weld residual stresses: numerical study and neutron diffraction measurement. Mater Des 2018;147:65–79.
[44] Zhang Y, Ying Y, Liu X, Wei H. Deformation control during the laser welding of a Ti6Al4V thin plate using a synchronous gas cooling method. Mater Des 2016;90:931–41.
[45] Li M, Ji S, Yan D, Yang Z. Controlling welding residual stress and distortion by a hybrid technology of transient thermal tensioning and trailing intensive cooling. Sci Technol Weld Join 2019;24:527–37.
[46] Martin O, De Tiedra P, Lopez M, San-Juan M, García C, Martín F, et al. Quality prediction of resistance spot welding joints of 304 austenitic stainless steel. Mater Des 2009;30:68–77.
[47] Chen B, Wang J, Chen S. Prediction of pulsed GTAW penetration status based on BP neural network and DS evidence theory information fusion. Int J Adv Manuf Technol 2010;48:83–94.
[48] Fu G, Gu J, Lourenco MI, Duan M, Estefen SF. Parameter determination of double-ellipsoidal heat source model and its application in the multi-pass welding process. Ships Offshore Struct 2015;10:204–17.
[49] Belitzki A, Marder C, Huissel A, Zaeh MF. Automated heat source calibration for the numerical simulation of laser beam welded components. J Inst Eng Prod 2016;10:129–36.
[50] Tafarroj MM, Kolahan F. A comparative study on the performance of artificial neural networks and regression models in modeling the heat source model parameters in GTA welding. Fusion Eng Des 2018;131:111–8.
[51] Hammad A, Churiaque C, Sánchez-Amaya JM, Abdel-Nasser Y. Experimental and numerical investigation of hybrid laser arc welding process and the influence of welding sequence on the manufacture of stiffened flat panels. J Manuf Process 2021;61:527–38.
[52] Bruna-Rosso C, Demir AG, Previtali B. Selective laser melting finite element modeling: validation with high-speed imaging and lack of fusion defects prediction. Mater Des 2018;156:143–53.
[53] Lee SH, Kim E, Park J, Choi J. Numerical analysis of thermal deformation and residual stress in automotive muffler by MIG welding. Journal of Computational Design and Engineering 2018;5:382–90.
[54] Jiang J, Chiew S, Lee C, Tiong P. A numerical study on residual stress of high strength steel box column. J Constr Steel Res 2017;128:440–50.
[55] Moslemi N, Gol Zardian M, Ayob A, Redzuan N, Rhee S. Evaluation of sensitivity and calibration of the chaboche kinematic hardening model parameters for numerical ratcheting simulation. Appl Sci 2019;9:2578.

[56] Moslemi N, Golzardian M, Redzuan N, Mozafari F, Ayob A. Optimization procedure for parameter determination of caboche kinematic hardening model. In: IOP conference series: materials science and engineering. IOP Publishing; 2020. 012112.
[57] Xu J, Gilles P, Duan Y, Yu C. Temperature and residual stress simulations of the NeT single-bead-on-plate specimen using SYSWELD. Int J Pres Ves Pip 2012;99:51–60.
[58] Zhao D, Wang Y, Liang D, Zhang P. Modeling and process analysis of resistance spot welded DP600 joints based on regression analysis. Mater Des 2016;110:676–84.
[59] Zhao D, Wang Y, Liang D, Ivanov M. Performances of regression model and artificial neural network in monitoring welding quality based on power signal. J Mater Res Technol 2020;9:1231–40.
[60] Marquardt DW. An algorithm for least-squares estimation of nonlinear parameters. J Soc Ind Appl Math 1963;11:431–41.
[61] Levenberg K. A method for the solution of certain non-linear problems in least squares. Q Appl Math 1944;2:164–8.
[62] Shakibjoo AD, Moradzadeh M, Moussavi SZ, Mohammadzadeh A, Vandevelde L. Load frequency control for multi-area power systems: a new type-2 fuzzy approach based on Levenberg–Marquardt algorithm. ISA transactions; 2021.
[63] Ranganathan A. The levenberg-marquardt algorithm. Tutoral on LM algorithm 2004;11:101–10.
[64] Croeze A, Pittman L, Reynolds W. Solving nonlinear least-squares problems with the Gauss-Newton and Levenberg-Marquardt methods. Portable Document format; 2012.
[65] Ebrahimzadeh A, Ghafari M, Moshkbar-Bakhshayesh K. Detection and estimation of faulty sensors in NPPs based on thermal-hydraulic simulation and feed-forward neural network. Ann Nucl Energy 2022;166:108726.
[66] Kim Y, Gu GH, Asghari-Rad P, Noh J, Rho J, Seo MH, et al. Novel deep learning approach for practical applications of indentation. Materials Today Advances 2022;13:100207.
[67] Guo T, Pan K, Sun B, Wei L, Yan Y, Zhou Y, et al. Adjustable Leaky-Integrate-and-fire neurons based on memristor-coupled capacitors. Materials Today Advances 2021;12:100192.
[68] Luo Y, Liu J, Xu H, Xiong C, Liu L. Regression modeling and process analysis of resistance spot welding on galvanized steel sheet. Mater Des 2009;30:2547–55.
[69] Dutta P, Pratihar DK. Modeling of TIG welding process using conventional regression analysis and neural network-based approaches. J Mater Process Technol 2007;184:56–68.
[70] Obeid O, Alfano G, Bahai H, Jouhara H. Numerical simulation of thermal and residual stress fields induced by lined pipe welding. Therm Sci Eng Prog 2018;5:1–14.
[71] Hemmesi K, Farajian M, Boin M. Numerical studies of welding residual stresses in tubular joints and experimental validations by means of x-ray and neutron diffraction analysis. Mater Des 2017;126:339–50.
[72] Tn TN. Measurement of residual stresses by the hole-drilling* strain gage method. 1993.